Proceedings of ASME Turbo Expo 2019: Turbomachinery Technical Conference & Exposition
GT2019
June 17-21, 2019, Phoenix, Arizona, USA

GT2019-91870

HEAT TRANSFER COEFFICIENT AUGMENTATION FOR A SHAPED FILM COOLING HOLE AT A RANGE OF COMPOUND ANGLES

Shane Haydt
Pratt & Whitney
United Technologies Corporation
East Hartford, CT, USA

Stephen Lynch
Department of Mechanical Engineering
Pennsylvania State University
University Park, PA, USA

ABSTRACT

Shaped film cooling holes are used to efficiently deliver coolant to the surface of a gas turbine part to keep metal temperatures low. The ultimate goal of film cooling is to reduce the heat flux into a component, relative to a case with no coolant injection. This reduction in heat flux is primarily achieved via a lower driving temperature at the wall for convection, represented by the adiabatic effectiveness. Another important consideration, however, is how the disturbance to the flowfield and thermal field caused by the injection of coolant augments the heat transfer coefficient. The present study examines the spatially-resolved heat transfer coefficient augmentation for a shaped film cooling hole at a range of compound angles, using a constant heat flux foil and IR thermography. Results show that the heat transfer coefficient increases with compound angle and with blowing ratio. Due to the unique asymmetric flowfield of a compound angle hole, a significant amount of augmentation occurs to the side of the film cooling jet, where very little coolant is present. This causes local regions of increased heat flux, which is counter to the goal of film cooling. Heat transfer results are compared with adiabatic effectiveness and flowfield measurements from a previous study.

INTRODUCTION

There are many parameters which can influence the performance of a shaped film cooling hole, such as the size and shape of the diffuser. The optimal parameters will reduce the jet momentum and keep the coolant attached to the wall with a significant lateral spread. In such a configuration, the film cooling hole would decrease the heat flux into the part because of the high coolant concentration on the surface and therefore decrease the driving temperature difference for convection heat transfer between the metal and the air. However, the temperature difference is just one component of the convective heat flux equation. The adjustment of film cooling hole parameters can also affect the convective heat transfer coefficient, h_f, due to a change in the temperature gradient at the wall, which is closely tied to the fluid dynamics of the flow.

For a surface with no film cooling, the equation to describe convective heat flux is,

$$q_0" = h_0 * (T_w - T_\infty) \qquad Eq.\ 1$$

where T_w is the wall temperature, T_∞ is mainstream temperature, and h_0 is the convective heat transfer coefficient, which describes the temperature gradient of the flat plate boundary layer.

The addition of film cooling complicates this equation, because T_∞ is no longer the driving temperature due to the presence of the coolant jet, and h_0 no longer accurately describes the temperature gradient at the wall. An equation specifically describing the heat flux for film cooling can be defined as,

$$q_f" = h_f * (T_w - T_{aw}) \qquad Eq.\ 2$$

where T_{aw} is the adiabatic wall temperature and h_f is the convective heat transfer coefficient that describes the convection of heat due to the fluid dynamics in the presence of film cooling. Note that this formulation assumes that h_f is independent of temperature.

Eq.'s 1 and 2 can be combined in order to show the net heat flux reduction due to the presence of film cooling,

$$NHFR = 1 - \frac{q_f"}{q_0"} = 1 - \frac{h_f}{h_0}\left(1 - \frac{\eta}{\phi}\right) \qquad Eq.\ 3$$

which can be represented in terms of three non-dimensional quantities: heat transfer coefficient (HTC) augmentation (h_f/h_0), adiabatic effectiveness (η), and non-dimensional metal temperature (ϕ). The present study directly measures HTC augmentation by using IR thermography and a constant heat flux thin foil heater. Adiabatic effectiveness for the same cases was measured in a previous study (Haydt and Lynch [1]), and non-dimensional metal temperature was assumed to be a uniform value of ϕ=0.6, which is convention [2].

HTC augmentation is generally considered to be small or negligible for shaped film cooling holes, and it is therefore not often studied or reported, so the effect of many film cooling hole design parameters on HTC augmentation is not well known. One parameter that is of particular interest in this study is the

compound angle (CA) of a shaped film cooling hole, since an increasing compound angle creates an asymmetric flowfield with a strong streamwise vortex located on the side of the coolant jet (Haydt and Lynch [3]). This study examines the HTC augmentation of the 7-7-7 hole, developed by Schroeder and Thole [4], (shown in Figure 1) at a sweep of compound angles (shown in Figure 2), and compares those results to adiabatic effectiveness from [1] and flowfield data from [3]. The naming convention for the holes is CA#, where the number (#) designates the compound angle relative to the x-direction.

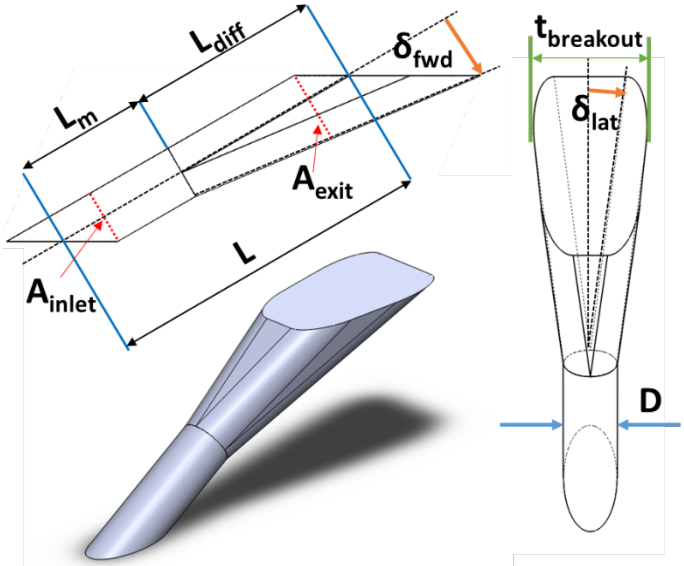

Figure 1: 7-7-7 public shaped film cooling hole developed by Schroeder and Thole [4].

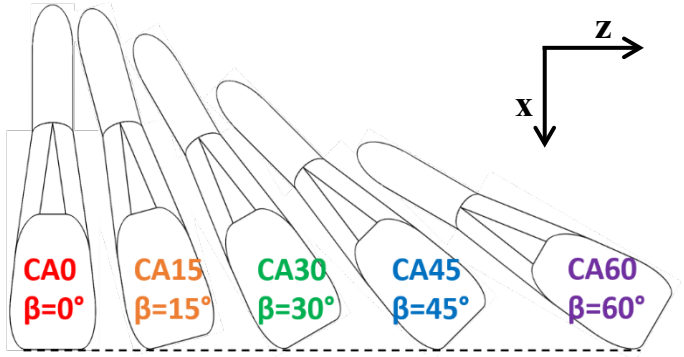

Figure 2: The 7-7-7 hole at the sweep of compound angles tested in this study.

NOMENCLATURE

A	hole cross-sectional area
AR	area ratio, A_{exit}/A_{inlet}
c_f	skin friction coefficient
D	diameter of film cooling holes
DR	density ratio, ρ_c/ρ_∞
h	convective heat transfer coefficient
H	shape factor, δ^*/θ
I	electric current
IR	momentum flux ratio, $\rho_c U_c^2/\rho_\infty U_\infty^2$
k	thermal conductivity
L	hole length
$\dot{m}_c$	coolant mass flow rate
M	blowing ratio, $\rho_c U_c/\rho_\infty U_\infty$
Nu_x	local Nusselt number, $Nu_x = hx/k$
p	static pressure
P	pitch, lateral distance between holes
q"	local heat flux
q_s"	local surface heat flux, $q_s" = VI/A_{heater}$
Re	Reynolds number ($Re^* = \delta * u_\tau/\nu_\infty$, $Re_\theta = U_\infty * \theta/\nu_\infty$, $Re_D = U_\infty * D/\nu_\infty$, $Re_c = U_c * D/\nu_c$)
$t_{breakout}$	hole breakout width
T	temperature
Tu	freestream turbulence intensity, u_{rms}/U_∞
U_∞	mainstream mean velocity
u_{jet}	coolant jet velocity in the direction of the metering section centerline
u_τ	friction velocity, $U_\infty\sqrt{c_f/2}$
V	electric voltage
$\lvert V \rvert$	velocity magnitude
x	downstream distance measured from hole trailing edge
y	vertical distance from surface
z	spanwise distance measured from center hole
z'	spanwise distance measured from the point of maximum effectiveness for each jet

Greek

α	hole injection angle
β	compound angle
δ	expansion angle for diffuser
$\delta\eta$	experimental uncertainty in effectiveness
$\delta\eta_b$	bias uncertainty in effectiveness
δ_t	thermal boundary layer thickness
δ^*	displacement thickness
δ_{99}	99% boundary layer thickness
ε	emissivity
η	local adiabatic effectiveness, $(T_\infty - T_{aw})/(T_\infty - T_c)$
θ	momentum thickness, or non-dimensional wall temp
ν	kinematic viscosity
ρ	fluid density
σ	Boltzmann constant, $\sigma = 5.67 * 10^{-8}\ W/m^2K^4$
ϕ	non-dimensional wall temp., $(T_w - T_\infty)/(T_\infty - T_c)$

Subscripts

0	flat plate conditions with no film cooling
aw	adiabatic wall
b	breakout
c	coolant, at hole inlet
diff	diffuser
exit	exit plane of the film cooling hole
f	in the presence of film cooling
fwd	forward expansion of diffuser
inlet	inlet plane of the film cooling hole
lat	lateral expansion of the diffuser

m	metering section
w	wall
∞	mainstream

Superscripts

¯	laterally-averaged
=	area-averaged

REVIEW OF RELEVANT LITERATURE

Film cooling is an external cooling methodology that has been studied quite extensively, particularly with regard to its adiabatic effectiveness. It is well established that film cooling holes with the addition of a shaped diffuser improve adiabatic effectiveness, especially at higher blowing ratios, which is evident from the review of shaped film cooling hole research done by Bunker [5]. Also evident from this review is that most of the research done on film cooling has been primarily focused on adiabatic effectiveness, as it is assumed this has the largest influence on the reduction of the heat load to a film-cooled part. Another variable that can influence the heat flux due to film cooling is the heat transfer coefficient (HTC) augmentation.

HTC augmentation has been measured by Goldstein et al. [6], Hay et al. [7], and Ammari et al. [8] for cylindrical holes using a naphthalene sublimation technique employing the heat/mass transfer analogy. All three studies found a 15-40% increase in laterally-averaged heat transfer coefficient immediately downstream of the hole trailing edge for blowing ratios of M=1.0 and 2.0. Baldauf et al. [9] found similar data at these same conditions using an alternate measurement technique; surface temperature was measured using infrared thermography on a heated testplate, and heat transfer coefficient was calculated based on a finite element model of the testplate, using the surface temperature and embedded thermocouples beneath the plate as boundary conditions. A final measurement technique for heat transfer coefficient is using a thin constant heat flux foil and measuring the ensuing surface temperature in flow that has equal coolant and mainstream temperature. This setup was used by Harrison et al. [10] to find the HTC augmentation from baseline cylindrical holes and holes embedded in a trench. A unique feature of this study was that heating upstream of the holes was considered, and Harrison et al. found that with the presence of upstream heating, the HTC augmentation due to film cooling increases by about 100%. This setup is also more reflective of the environment on a turbine airfoil surface, where the velocity and thermal boundary layers would develop together.

HTC augmentation has also been studied for shaped holes, but there is not very good agreement in the results. Gritsch et al. [11] and Yu et al. [12] both reported that shaped holes had lower HTC augmentation than cylindrical holes, especially at high blowing ratios. Even further, these studies suggest that shaped holes reduce the heat transfer coefficient relative to a flat plate with no cooling, because the low momentum coolant thickened the boundary layer. Alternately, Saumweber and Schulz [13] and Boyd et al. [14] both showed that shaped holes have significant HTC enhancement relative to a flat plate, and higher augmentation than for cylindrical holes [13]. Bunker [5] suggested that this disparity that exists in HTC augmentation studies is due to the relative thickness of the incoming boundary layer, with "thick" boundary layers of $\delta/D > 0.5$ experiencing a reduction in HTC with film cooling injection, and "thin" boundary layers of $\delta/D < 0.15$ experiencing an increase in HTC. However, all of the aforementioned studies have what Bunker classifies as "thick" boundary layers. It is also worth noting that none of the aforementioned studies employ upstream heating. Clearly, more research into shaped hole HTC augmentation is needed.

The region in which high augmentation occurs for streamwise-oriented holes is immediately downstream of the hole outlet. There is also high levels of adiabatic effectiveness in this region, and therefore the increased heat transfer coefficient would not have a significant effect on the heat flux into the part. This is largely why research on HTC augmentation is not prioritized. However, for compound angled holes, the regions of high HTC augmentation do not necessarily correspond with regions of high effectiveness. Sen et al. [2] introduced the concept of Net Heat Flux Reduction (NHFR), or the ratio of reduction in heat transfer with film cooling to the heat transfer without film cooling. This helps quantify the combined effects of HTC augmentation and adiabatic effectiveness.

In a compound angled film cooling hole, the mainstream flow wraps over and around the coolant jet, creating a strong shear layer on the leeward side, which rolls up to become a strong streamwise vortex [3]. High compound angles enable higher blowing ratios, and provide a wide lateral spread of coolant, which leads to high adiabatic effectiveness levels that decay slowly with increasing blowing ratio [1]. As the compound angle increases from zero, the flowfield changes from a counter-rotating vortex pair and becomes increasingly asymmetric as the streamwise vortex dominates the flowfield [3]. It is reasonable to assume that the HTC augmentation also changes with compound angle, since it is so closely tied to the flowfield.

Aga and Abhari [15] found that the HTC increases as compound angle increases for cylindrical holes, and also there is a region of high augmentation adjacent to the jet, due to the influence of the streamwise vortex. Due to this increase, particularly in a region without high coolant concentration, NHFR decreased with compound angle and with blowing ratio, and was even negative at a momentum flux of IR=3 [15]. Sen et al. [2] found similar results for compound angled shaped holes. HTC increased and NHFR decreased with increasing blowing ratio for a shaped hole at a compound angle of 60˚. However, there was no comparison to a shaped hole oriented in the streamwise direction. Brauckmann and von Wolfersdorf [16] measured the HTC for shaped holes at a compound angle of 0˚ and 45˚, and HTC increased with compound angle and with blowing ratio, particularly downstream. Contour plots of HTC augmentation indicate that much of the increase in HTC was due to the influence of the streamwise vortex, in the region adjacent to the jet. Recently, Anderson et al. [17] and McClintic et al. [18] examined the effects of freestream conditions and internal crossflow velocity on the HTC augmentation for a 45˚ 7-7-7

hole. Greater HTC augmentation was present for a lower freestream turbulence intensity of Tu=0.5%, as compared to Tu=4.5%, for approach flows with the same boundary layer thickness [17]. Also, film cooling injected into a laminar boundary layer had very significant HTC augmentation [17]. An in-line crossflow condition caused an increase in HTC augmentation as compared to a counter crossflow condition [18].

The present work is the first of its kind to examine the HTC augmentation on a compound angled shaped hole (CASH) for a sweep of compound angles, in order to see how the magnitude and location of HTC augmentation changes as compound angle increases. Additionally, since the impact of upstream heating was so significant [10], this study is unique in its uninterrupted heater foil, which extends from 40 diameters upstream to 40 diameters downstream, with the hole outlets cut out.

EXPERIMENTAL SETUP

A schematic of the test facility used for the present study is shown in Figure 3. This is a closed-loop, recirculating wind tunnel facility with a mainstream loop and coolant loop, which are kept isothermal for this particular test. The mainstream flow is driven by an axial fan, and its temperature is measured by four thermocouples on a probe located directly upstream of the film cooling holes. The secondary coolant loop draws air from the mainstream flow via a hermetically sealed blower, and the temperature is monitored via eight thermocouples in the plenum. The velocity is measured via Pitot probe in the test section and the mass flow is measured with a Venturi in the coolant loop to set the blowing ratio. The density ratio for all cases in this study was 1.0.

At the entrance to the test section, a suction loop removes the incoming boundary layer, allowing a new one to form on the low-conductivity Styrofoam endwall (k=0.029 W/m-K). The boundary layer transitions to turbulence due to a trip wire located 40 diameters upstream of the film cooling hole leading edge. The hydrodynamic boundary layer for this facility was measured by Schroeder and Thole [4] at a location of x/D= -5.4 and the reported average values are Tu=0.5%, δ/D=1.4, θ/D = 0.16, H = 1.45, Re_θ = 670, Re* = 315, Re_D=3,800 and u_τ = 0.5 m/s.

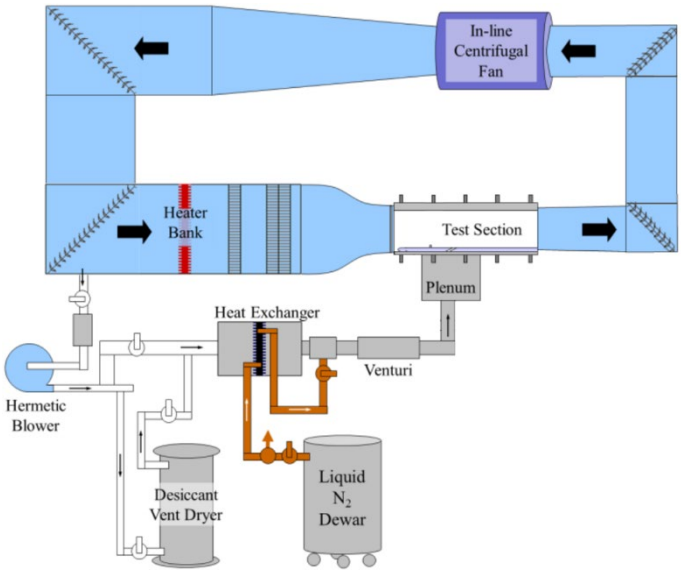

Figure 3: Closed-loop wind tunnel facility used in the present study.

Surface temperatures on the heater foil surface covering the endwall are measured with a FLIR T650sc infrared camera. Images are taken at an angle through an infrared transmissible ZnSe window, and are dewarped using an in-house MATLAB code. Temperatures are corrected via an in-situ IR calibration. The average deviation between the surface thermocouples and the IR camera reading from the calibration is ±1.3˚ C.

Heat transfer coefficient measurements were taken by measuring the surface temperature of a thin foil heater, made of 0.001" thick hardened 304 stainless steel supplied with electrical current. The upstream edge of the heater foil was attached to a copper bus-bar using conductive silver epoxy, and the downstream edge was clamped between two copper bars. The heater foil was attached to the low-conductivity Styrofoam endwall using 3M VHB insulating tape (k=0.16 W/m-K) with a thickness of 0.020". A cross section of the heater setup is shown in Figure 4a, not to scale. The foil was slowly rolled out onto the tape to prevent air pockets and ensure aerodynamic smoothness. After the attachment of the foil, three thin layers of black spray paint, with emissivity of ε = 0.965 reported by the manufacturer, were applied to the heater. The electrical current through the foil resulting in Joule heating is provided by a DC power supply, which provided a current of 48 A. Voltage across the heater was measured using a multimeter. This setup was capable of providing a heat flux of 1050 W/m^2. When the film hole exits were cut out, great care was taken to ensure there was no forwards or backwards facing step at the leading edge and trailing edge, which is indicated in the figure.

The heater foil, shown in Figure 4b, extended from -39.5 diameters upstream of the hole leading edge to about 40 diameters downstream of the trailing edge. The beginning of the foil is just downstream of the boundary layer trip, so thermal and velocity boundary layers are able to grow over the same distance.

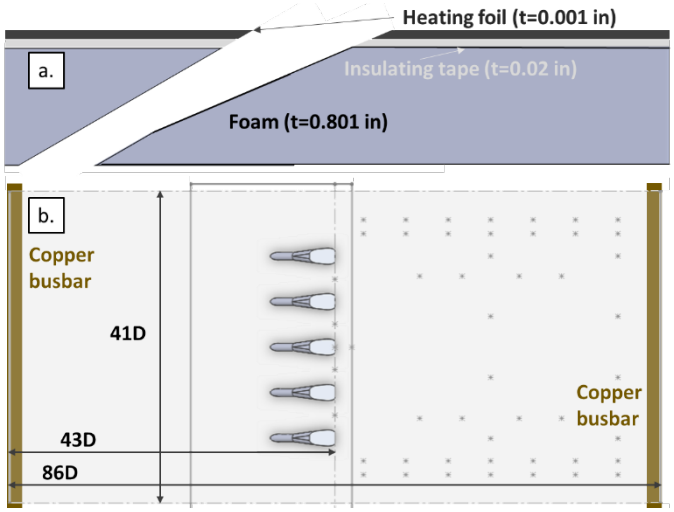

Figure 4: (a) A cross section view of the heater attachment (not to scale), (b) a schematic of the heater foil, showing the copper busbars, location of the holes, and downstream dots used for image correction.

Although the thermal boundary layer was not directly measured in this study, the measured flat plate heat transfer coefficient over the smooth heater (without hole cutouts) agreed very well to a correlation for an equilibrium turbulent boundary layer with a virtual origin at the trip location. Figure 5 shows a comparison of the laterally-averaged Nusselt number versus x/D, where the lateral averaging is performed over a lateral extent corresponding to each of the five holes in the tunnel (although no holes are physically present). For all five pitchwise regions on the heater, the agreement to a fully turbulent boundary layer correlation is within 2%. The thermal boundary layer thickness at x/D= -5.4 is expected to be $\delta_t/\delta \approx 1$ (since the flow is turbulent), and thus $\delta_t/D=1.4$. Relative to the gas turbine environment, this upstream heated condition is likely most relevant to film rows on the aft pressure side, downstream of the leading edge.

Three tests are needed to calculate the heat transfer coefficient. First, a flat plate test with no film cooling holes is completed and compared to a turbulent boundary layer correlation to confirm the validity of the foil installation, and also to check for lateral uniformity. Next, the holes are carefully cut out of the foil using a mask, so that only the foil inside of the hole's edges is removed. This does locally change the current concentration in the foil, and thus the uniformity of surface heat flux. This is accounted for by blocking the holes with clay such that no air can exit and the surface is aerodynamically smooth. A second flat plate test is then compared to the results from the first test in order to determine local heat flux. Finally, with the holes cut out and unblocked, a sweep of blowing ratios is run, from M=1.0 to 4.0.

To calculate heat transfer coefficient, a Matlab script takes all of the images from the aforementioned three tests and calculates the following:

First, the flat plate, no hole cutout surface temperature measurements are used to calculate the flat plate heat transfer coefficient (Figure 6a) using Eq. 4

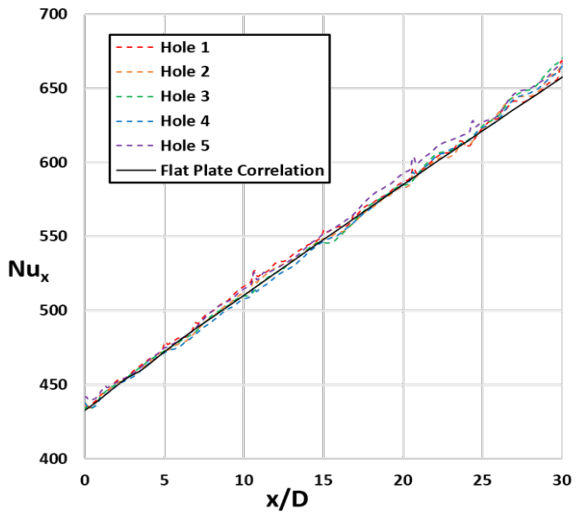

Figure 5: Laterally-averaged local Nusselt number versus distance downstream for the smooth plate, compared to a fully turbulent flat plate correlation.

$$h_0(x,z) = \frac{1}{(T_s(x,z)-T_\infty)}\left[\frac{V*I}{A} - \varepsilon\sigma\left(\left(T_s(x,z)\right)^4 - T_\infty^4\right)\right] \quad Eq.\ 4$$

where the first term inside the brackets in Eq. 4 is the electrical power dissipated by the heater, and the second term is a local correction for radiation. At cooler spots on the foil, radiation accounted for only 5% of the total heat flux, but at the hottest spots, it accounted for about 25%. All calculations involving heat flux were corrected for radiation. Conduction losses were estimated to be a maximum of 2% of heat flux at the regions of highest temperature, but are less than 1% for almost all regions of the foil.

The next calculation step is to determine local heat flux (Figure 6b) due to the change in current concentration created by cutting out the holes, using Eq. 5. The surface temperature from the flat plate, blocked holes case is used as T_s in this calculation, and it is assumed that the flat plate heat transfer coefficient (Figure 6a) is the same locally since the plate is still aerodynamically smooth, and the test is run at the same mainstream conditions.

$$q_s''(x,z) = h_0(T_s(x,z) - T_\infty) + \varepsilon\sigma\left(\left(T_s(x,z)\right)^4 - T_\infty^4\right) \quad Eq.\ 5$$

Aside from the current concentration, there is one other slight difference in the wall boundary condition, which is that there is now an unheated portion of the wall over the film cooling hole outlet. An estimation for how this might alter the local flat plate heat transfer coefficient downstream of the hole was done using the expression for surface temperature resulting from

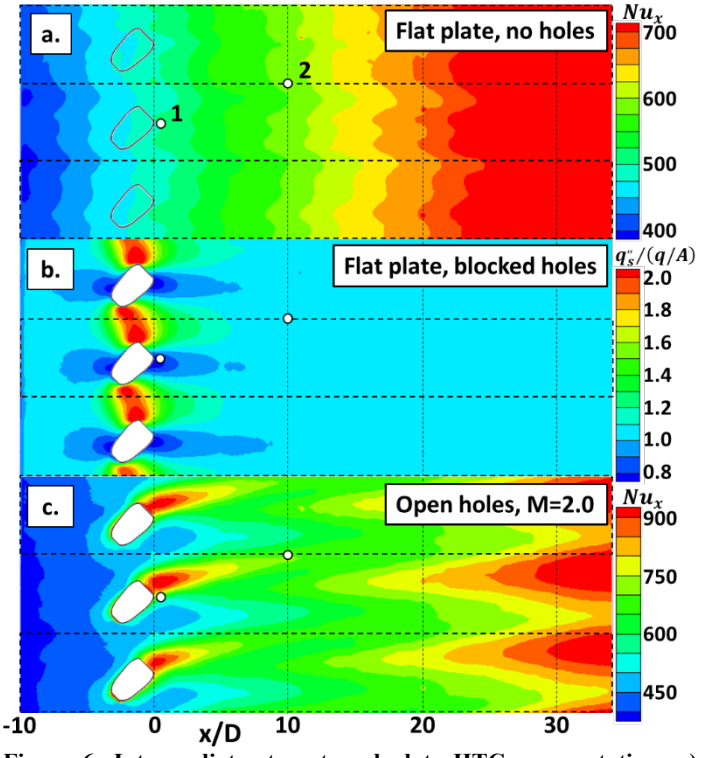

Figure 6: Intermediate steps to calculate HTC augmentation: a) Local Nusselt number calculated from flat plate with no holes cut out; b) Local heat flux (normalized by overall supplied power), for a case with holes cut out of the foil but blocked from flowing; c) Local Nusselt number for flowing holes calculated using local heat flux.

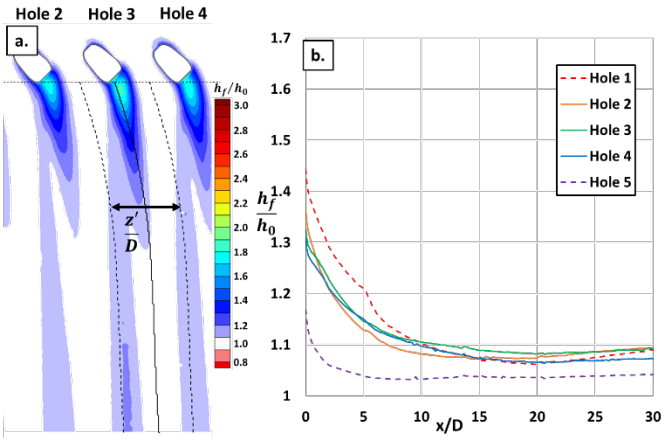

Figure 7: a) Contours of HTC augmentation for the CA45 hole at M=2.0, showing repeatability of the center three holes. b) Curves of laterally-averaged HTC augmentation for the CA45 hole at M=2.0, showing good periodicity for the center three holes

constant free-stream velocity flow along a semi-infinite plate with arbitrarily specified heat flux, from Kays and Crawford [19]. It was found that the heat transfer coefficient could be increased by 2.8-3.6 W/m^{2}K just downstream of the hole outlet, depending on hole orientation. Holes with a longer total unheated distance in the x-direction (CA0-CA30) have a higher increase, which accounts for about 9% of the local flat plate HTC. Holes with a shorter x-distance would only have an increase of 7% in the local flat plate HTC. Also, a significant portion of the flow travels at the midpitch between the holes which would not have an unheated length. Mixing between these two streams also likely decreases this effect.

Local heat flux is different for all CA cases, since the different orientations of the hole outlets change the current concentration. Figure 6b shows the local heat flux for a CA45 hole. The heat flux is identical, however, for each blowing ratio case for a given hole orientation (the temperature change in the foil with coolant is <15°C over all blowing ratio cases, which does not change the foil resistivity appreciably). Therefore, the final step is to apply this local heat flux to the different blowing ratio case images, using Eq. 6:

$$h_f(x,z) = \frac{1}{(T_s(x,z)-T_\infty)}\left[q_s''(x,z) - \varepsilon\sigma\left(\left(T_s(x,z)\right)^4 - T_\infty^4\right)\right] \quad Eq.\ 6$$

This final step results in local HTC measurements for each blowing ratio case. An example for CA45, M=2.0 is shown in Figure 6c. Results in this paper are presented in terms of the HTC augmentation, h_f/h_0, which is the local values of Figure 6c divided by those in Figure 6a, shown in a laterally-averaged sense in Figure 7.

UNCERTAINTY ANALYSIS

The experimental uncertainty was found for flat plate HTC, local heat flux, and HTC augmentation by using the propagation of measurement uncertainties analysis [20]. Uncertainties in all measured quantities are driven primarily by the bias uncertainty of the surface temperature, which is 1.4˚ K. This is the combined uncertainty from the thermocouples (±0.5˚ K) and the variation in the IR calibration (±1.3˚ K). Uncertainty also varies across the plate based on local temperature, so the uncertainty for two locations is presented. Point 1 in Figure 6 is located just downstream of the trailing edge, and Point 2 in Figure 6 is 10 diameters downstream at the midpitch. The uncertainty in flat plate HTC is the same for Points 1 and 2, and is ±2.4 W/m^{2}K, which is 5% of the mean HTC value on the foil heater. The flat plate HTC is used to calculate local heat flux, based on surface temperature measurements of the foil with holes cut out and blocked, so the uncertainty in that measurement propagates. The uncertainty in local heat flux is ±74 W/m^2 at Point 1 and ±72 W/m^2 at Point 2, which is 10% and 6.8% of local heat flux, respectively. Finally, that heat flux measurement is used to calculate HTC augmentation, so the uncertainty once again propagates. Uncertainty in h_f is ±8.0 W/m^{2}K at Point 1, which translates to an 11% uncertainty in h_f/h_0. At Point 2, the uncertainty is ±4.1 W/m^{2}K, or an 8% uncertainty in h_f/h_0.

When the heater foil is applied, before the holes are cut out, the foil has good lateral uniformity (<3% variation and standard deviation <1.3%) and agrees well with the flat plate correlation for a turbulent boundary layer (see Figure 5). Once the holes are cut out, there is good periodicity between the center three holes, as shown in Figure 7a and 7b for a CA45 hole at M=2.0. The augmentation for Holes 1 and 5 is not periodic, but this is because these holes are on the outside of the hole array and influenced by the wall and the edge of the heater foil. However, the jets from these holes provide periodic boundary conditions for the three holes in the center. The laterally-averaged results that are plotted in the results section below are the average of the three center holes. Also, a CA60 hole was tested, removed from the tunnel, re-installed and re-tested to confirm repeatability. The maximum difference in HTC augmentation (h_f/h_0) was 0.034, which is within the uncertainty of the measurement.

Since there is such significant lateral motion of compound angled jets, the traditional method of laterally-averaging over a rectangular pitch downstream of the hole does not accurately capture the performance of each hole. Instead, the coolant jet's path was determined based on the maximum point of adiabatic effectiveness (from a prior study [1]) at each x/D location. The laterally-averaged effectiveness, HTC augmentation, and NHFR were then calculated by averaging over the width of a pitch centered at a given path location. That center point, or the point of maximum effectiveness, is z'/D=0. The path (defined based on adiabatic effectiveness) is shown in Figure 6a with a solid black line, and the region over which the data is averaged is indicated with dashed lines.

DISCUSSION OF RESULTS

Experimental results for HTC augmentation are presented for five compound angled shaped holes at DR=1.0 and M=1.0 to 4.0. First, the effect of blowing ratio is shown for a CA0 and CA60 hole. Next, the effect of compound angle on HTC augmentation is discussed. Using adiabatic effectiveness data from Haydt and Lynch [1], the effect of blowing ratio and compound angle on NHFR is shown. Finally, results are

discussed in terms of the flow features, using PIV data from Haydt and Lynch [3].

Effect of Blowing Ratio

As blowing ratio increases, the HTC augmentation due to a film cooling hole also increases, for both a streamwise oriented and compound angled hole. Figure 8 shows contours of HTC augmentation for the CA0 and CA60 holes at M=1.0 and M=4.0, with the white color band indicating no or negligible augmentation in heat transfer coefficient, as compared to a flat plate with identical freestream conditions. Contours indicate that the heat transfer coefficient is increased due to the presence of the cooling jet for all cases, particularly at the trailing edge of the hole. As blowing ratio increases, this trailing edge augmentation also increases, for both hole types. Further from the hole in the CA0, M=4.0 case, the heat transfer coefficient is increased by 10-40% by the presence of the jet, and that augmentation persists further downstream as the blowing ratio increases, due to the increasingly significant disturbance caused by the jet.

Figure 9 shows the laterally-averaged HTC augmentation for the two hole types shown in Figure 8, at all tested blowing ratios. This once again indicates that the augmentation increases as blowing ratio increases, particularly downstream of the hole, and this is true for both a streamwise oriented and compound angeld hole. HTC augmentation is likely increasing for two reasons: the injection of higher velocity flow near the endwall will thin the boundary layer and increase the velocity gradient at the wall, and also the jet-in-crossflow will lead to an increase in turbulent kinetic energy. Both of these effects are exacerbated by an increased blowing ratio.

An increase in heat transfer coefficient due to the presence of film cooling potentially decreases the usefulness of a film cooling hole, particularly if there is significant augmentation in a region where very little coolant is present. Figure 10 shows a plot of local adiabatic effectiveness from Haydt and Lynch [1] (right axis, solid lines) and local HTC augmentation (left axis, dashed lines), plotted versus pitchwise direction (z'/D) at x/D=5. A low blowing ratio of M=1.0 is shown in red lines, and a high blowing ratio of M=4.0 is shown in blue lines. Generally speaking, the regions of high augmentation correspond to regions of high to moderate coolant coverage. The high blowing ratio case, however, has a very narrow region of cooling

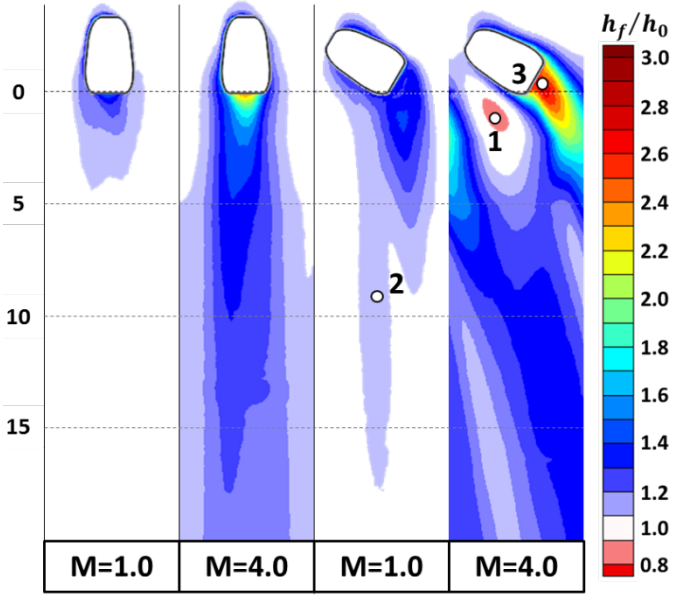

Figure 9: Contours of HTC augmentation for a CA0 and CA60 hole at M=1.0 and M=4.0.

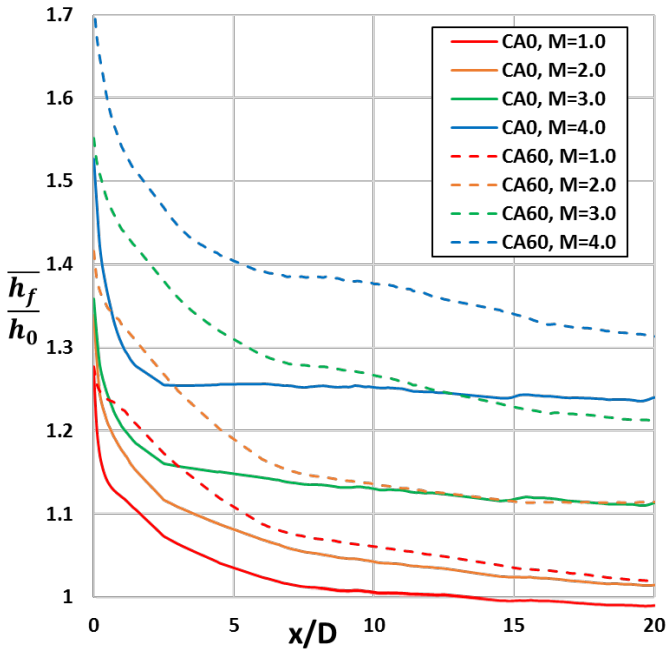

Figure 8: Laterally-averaged HTC augmentation for the CA0 and CA60 hole at a sweep of blowing ratios.

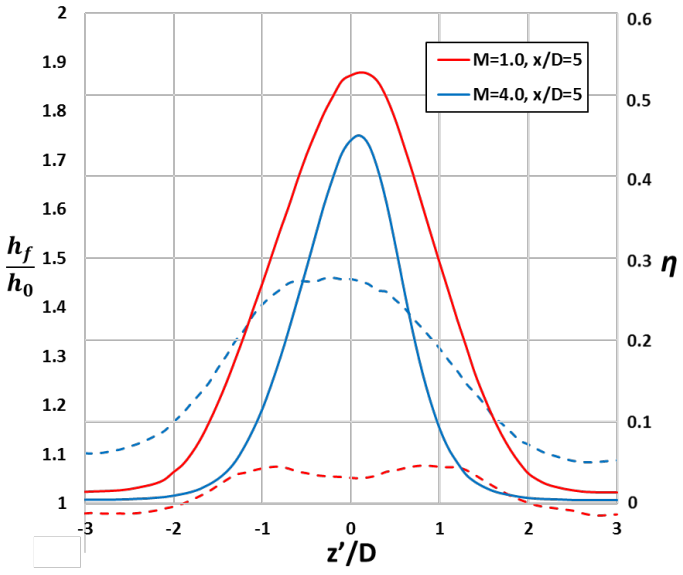

Figure 10: Local adiabatic effectiveness (right axis, solid lines) and HTC augmentation (left axis, dashed lines), at x/D=5 for the CA0 hole at a low and high blowing ratio.

effectiveness, but a wide region over which the heat transfer coefficient is increased.

Effect of Compound Angle

There are three interesting features of the HTC augmentation for the CA60 hole, and they can be explained by the asymmetric nature of the flowfield. Those features are indicated by points in Figure 8: 1. Decreased augmentation just downstream of the hole outlet, 2. Increased augmentation adjacent to the jet downstream, and 3. Increased augmentation immediately downstream of the trailing edge. Figure 11 shows a CFD prediction of the CA60 flowfield from Haydt and Lynch [3], with an isosurface of θ=0.2, the endwall contoured by adiabatic effectiveness, and streamlines indicating the direction of the flow. In a CASH flowfield, the compound angled injected jet poses as an asymmetric obstruction to the oncoming mainstream flow. The region just downstream of the hole outlet is thus shielded by this obstruction, and the velocity is reduced in this region. This thickens the boundary layer and decreases the heat transfer coefficient relative to a flat plate with no cooling, as indicated by Point 1 in cases M=2.0-4.0 in Figure 8.

In a CA60 flowfield, the mainstream flows over and around the jet, primarily on the leeward (right) side, creating a strong, asymmetric shear layer that rolls up to become a single streamwise vortex. The motion of the mainstream flow over the coolant jet is indicated by the streamlines in Figure 11, and also the lateral motion induced by the streamwise vortex. This vortex entrains mainstream fluid and impinges it on the surface in the region next to the jet. This effect is indicated in Figure 8 by Point 2. This streak of higher heat transfer coefficient due to the streamwise vortex can be seen for each case, starting around x/D=6, and its augmentation increases with blowing ratio.

The isosurface in Figure 11 indicates how a region of the coolant jet is wrapped up by the streamwise vortex and lifted up and away from the endwall. A lower momentum region of the coolant jet is able to trickle out of the trailing edge and remain attached to the wall, as indicated by the region of high effectiveness to the left of the hole outlet. This coolant increases the temperature and velocity gradient at the wall and leads to higher heat transfer augmentation as M increases.

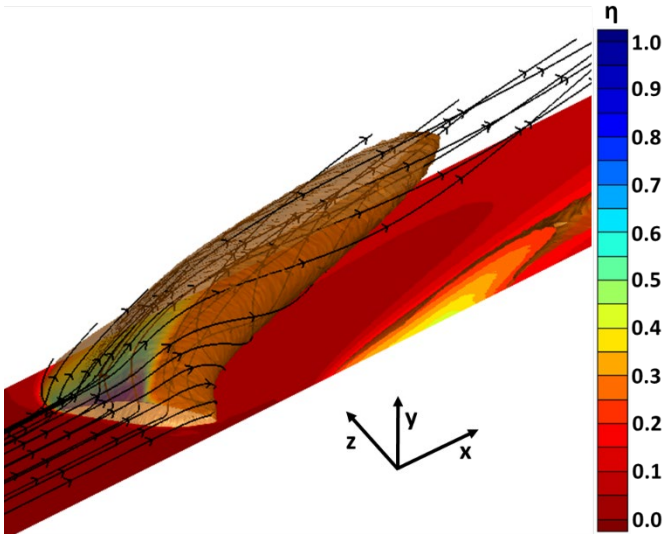

Figure 11: CFD prediction for a CA60 hole at M=3.0 [3]. Depicted with an adiabatic effectiveness contour on the endwall and an isosurface of nondimensional fluid temperature of θ =0.2.

The location of the streamwise vortex on the edge of the coolant jet poses a potential problem, which is that the heat transfer coefficient is being increased in a region where no or very little coolant exists. Figure 12 shows a plot of local adiabatic effectiveness (right axis, solid lines) and local HTC augmentation (left axis, dashed lines), plotted versus z'/D at x/D=5. A low blowing ratio of M=1.0 is shown in red lines, and a high blowing ratio of M=4.0 is shown in blue lines. Both blowing ratio cases have two peaks in augmentation: one near z'/D=0.5 which is due to the attached coolant thinning the boundary layer, and a second at z'/D=-1 for M=1.0, and z'/D=-2 for M=4.0, which is due to the downwash of the strong streamwise vortex. The low blowing ratio case has a good coolant spread across the entire pitch, and therefore does not have low effectiveness levels near these peaks in augmentation. The high blowing ratio case of M=4.0, however, has a narrower coolant jet footprint, and experiences a local decrease in effectiveness at z'/D=-2 which unfortunately aligns with a region of high heat transfer coefficient augmentation due to the streamwise vortex effect. The impact of this on the overall heat flux to the part is discussed in a later section.

As the compound angle of the 7-7-7 shaped hole increases, the flowfield transitions from a symmetric CRVP to an asymmetric streamwise vortex, and this change is reflected in the HTC augmentation. Figure 13 shows HTC augmentation contours for all compound angle cases at a blowing ratio of M=1.0. As the compound angle increases, the high augmentation region downstream of the hole outlet increases in size and magnitude. There is more significant lateral spread of attached coolant for higher compound angle holes [1], which

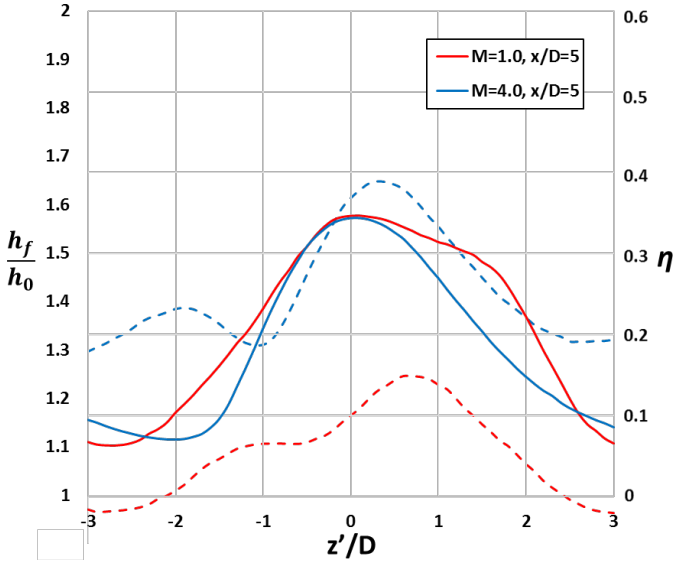

Figure 12: Local adiabatic effectiveness (right axis, solid lines) and HTC augmentation (left axis, dashed lines), at x/D=5 for the CA60 hole at a low and high blowing ratio.

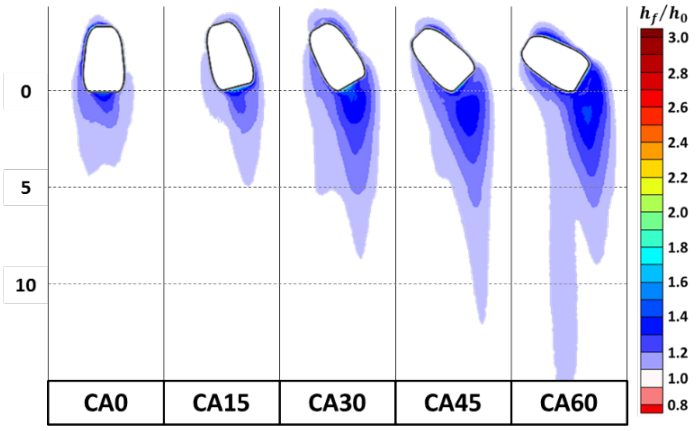

Figure 13: HTC augmentation contours for a sweep of compound angle holes at M=1.0.

increases its region of influence. Also, as the compound angle increases, the augmentation region far downstream of the hole due to the downwash of the streamwise vortex becomes more apparent.

Another interesting effect of increasing compound angle is an increased amount of augmentation at the upstream edge of the film cooling hole. As the coolant is ejected from the hole, it creates an obstruction to the mainstream flow. A computational study by Tyagi and Acharya [21], and an experimental study by Wright et al. [22], showed the development of a horseshoe vortex in front of a film cooling jet that arises due to the blockage of the jet causing a local separation of the boundary layer. As compound angle increases, the size of the obstruction increases, and therefore also the strength of the horseshoe vortex. This horseshoe vortex is highly unsteady, and also impinges mainstream gas on the surface, both of which lead to increased HTC augmentation.

For a higher blowing ratio of M=3.0, Figure 14 shows contours of HTC augmentation for a sweep of compound angles. First, the augmentation at the trailing edge increases with

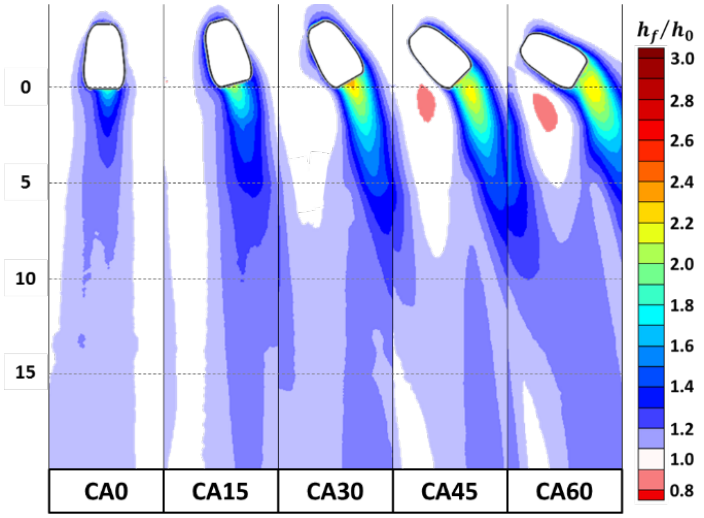

Figure 14: Contours of HTC augmentation for a sweep of compound angles at M=3.0.

compound angle, as attached coolant exiting the hole causes high velocity and temperature gradients at the wall which increase the local heat transfer coefficient. As discussed in Haydt and Lynch [1], increasing the compound angle of a shaped hole enables coolant to stay attached at higher blowing ratios. Additionally, the impact of the streamwise vortex on HTC augmentation downstream of the jet increases as compound angle increases. This region can be seen to the left of the jet in Figure 14, starting around x/D=6. Also, there is some augmentation on the upstream side of the compound angled film hole due to the horseshoe vortex caused by the obstruction of the coolant jet. Finally, the obstruction of the jet at high compound angles and high blowing ratio shields the region just downstream of the hole outlet from the mainstream flow, creating a region of reduced heat transfer.

Figure 15 shows local adiabatic effectiveness and HTC augmentation for the CA0, CA30, and CA60 holes at x/D=5 and M=3.0, plotted versus the z'/D coordinate system which is aligned with the jet path as defined by the maximum point of adiabatic effectiveness. For all three cases, the maximum peak in heat transfer augmentation occurs in the region where there is significant coolant. However, at this high blowing ratio of M=3.0, the signatures of the jets for all cases are fairly narrow (indicating detachment from the wall), and augmentation occurs in regions of low coolant concentration. For example, a local peak in augmentation due to the streamwise vortex exists at z'/D=-2 for the CA60 hole in Figure 15, which is a region of low effectiveness. Also, for CA30 at z'/D=-1.5, the heat transfer augmentation is increased by 5% above CA0, but the cooling effectiveness is the same for CA30 and CA0. These situations could potentially lead to a local increase in heat flux with the current film cooling scheme.

For the two blowing ratios shown here, and also for all blowing ratios tested, HTC augmentation increases with increasing compound angle. The area-averaged HTC

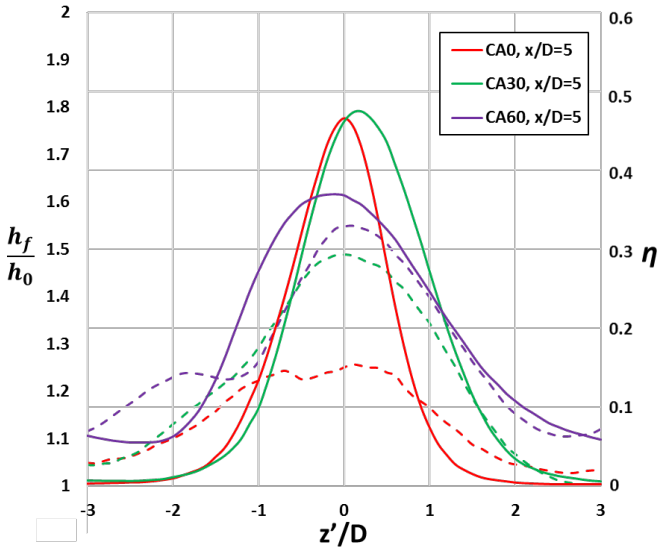

Figure 15: Local adiabatic effectiveness (right axis, solid lines) and HTC augmentation (left axis, dashed lines), at x/D=5 for the CA0, CA30, and CA60 holes at M=3.0.

augmentation (averaged from x/D=3 to 15, and over the three central hole trajectories from z'/D=±9) is shown in Figure 16a, with the area-averaged adiabatic effectiveness [1] shown in Figure 16b for comparison. Figure 16a shows a monotonic increase in HTC augmentation with compound angle and also with blowing ratio.

Net Heat Flux Reduction

As indicated in Eq. 3, the change in heat flux due to the presence of film cooling (NHFR) can be represented as a function of three variables: adiabatic effectiveness (η), HTC augmentation (h_f/h_0), and non-dimensional metal temperature (ϕ). A positive value of NHFR indicates that local heat flux has been reduced due to the presence of film cooling, and the higher the value, the larger the reduction. A negative value of NHFR indicates an increase in heat flux to the surface, which is obviously counter to the goals of film cooling. Two of the variables comprising Eq. 3 have been measured and presented in this paper, and the related paper by Haydt and Lynch [1], and ϕ is traditionally assumed to be 0.6. Note that the density ratios are slightly different between the HTC augmentation (DR=1.0) and the adiabatic effectiveness results [1] (DR=1.2). However, this is not expected to change the jet trajectory in a significant way; furthermore, NHFR is generally a qualitative metric, since the assumption of a uniform non-dimensional metal temperature (ϕ) is not accurate close to film cooling holes, or for varying blowing ratios. Figure 17 is a depiction of how effectiveness and augmentation can influence NHFR. For the CA30 hole at M=3.0, three contours are shown. First, a contour of adiabatic effectiveness. Second, a contour of HTC augmentation, overlaid with line contours of effectiveness. Third, a contour of NHFR, where a contour level of white indicates no change in heat flux, and pink contours indicate a negative NHFR, or rather an increase in heat flux.

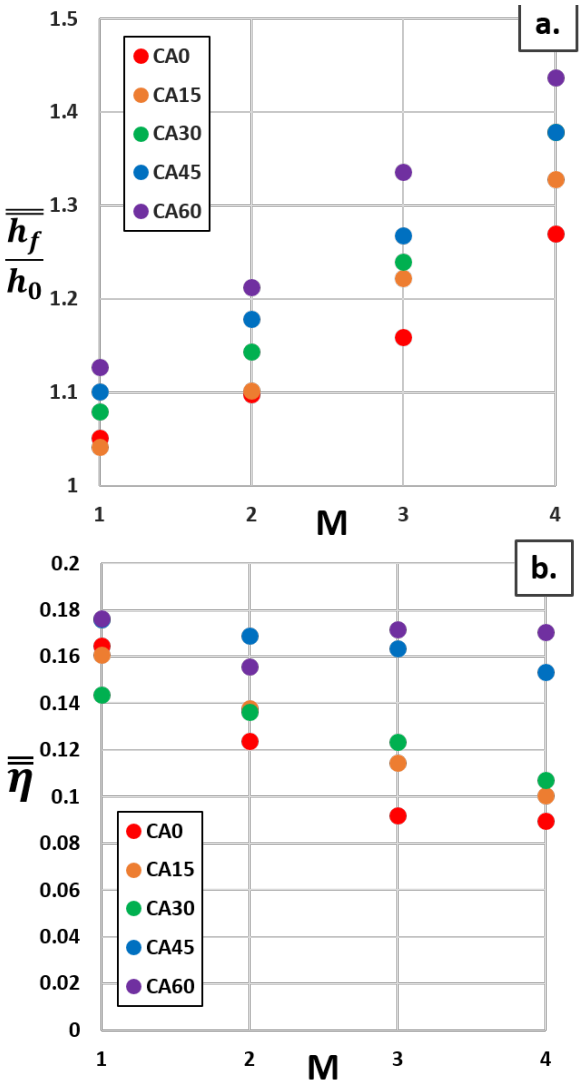

Figure 16: a.) Area-averaged HTC augmentation (DR=1.0) and b.) area-averaged adiabatic effectiveness (DR=1.2) [1] (from x/D=3 to 15) for all tested cases, plotted versus blowing ratio.

Contour lines of effectiveness overlaid on the augmentation contour plot show that the lowest level of effectiveness (η<0.1) exists in a region between the jets where the augmentation is high due to the streamwise vortex. The contour of NHFR shows that this combination of low effectiveness and high augmentation leads to a negative NHFR downstream of x/D=5. Alternately, even though the levels of heat transfer augmentation are very high near the trailing edge of the hole, the effectiveness levels are also very high, so the NHFR in this region is very high and the part would be cooler with film cooling.

The next figures present only NHFR, but are a combination of the HTC augmentation results presented above and also adiabatic effectiveness results from Haydt and Lynch [1].

Figure 18a shows contours of NHFR for a sweep of compound angles all at a low blowing ratio of M=1.0. Downstream of the hole, there are no areas of negative NHFR. At this low blowing ratio, a large amount of coolant remains attached to the wall and spreads out laterally. Even in areas of

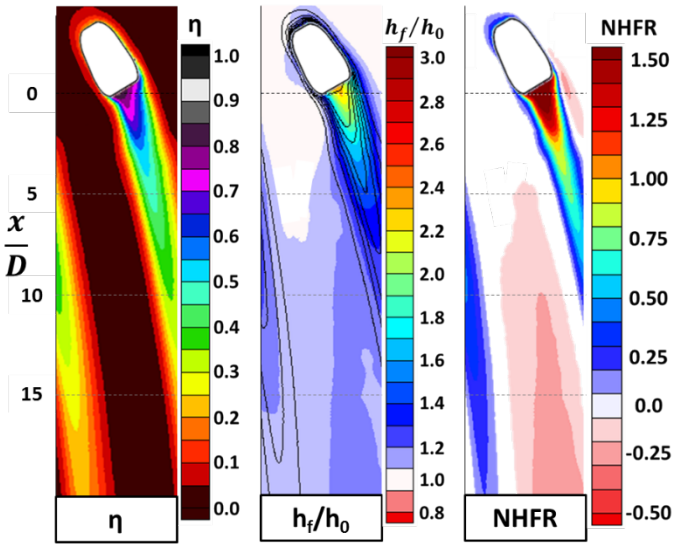

Figure 17: Contour plots of (from left to right) adiabatic effectiveness, HTC augmentation overlaid with adiabatic effectiveness line contours, and net heat flux reduction (NHFR) for the CA30 hole at M=3.0.

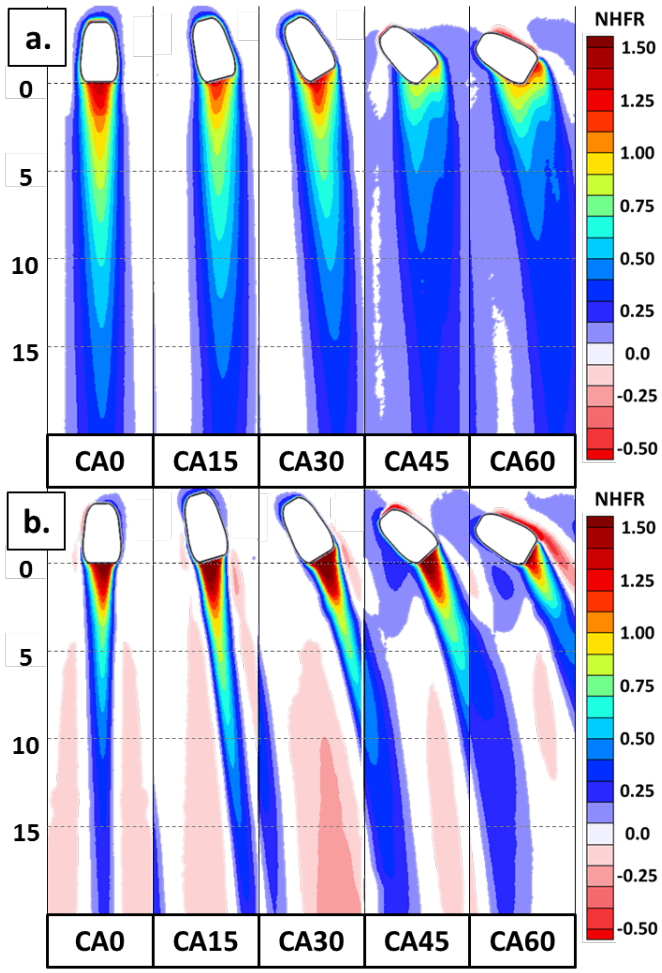

Figure 19: a) NHFR for a sweep of compound angles at M=1.0, and b) M=3.0.

high HTC augmentation (which can be seen in Figure 13), there is a significant level of coolant to maintain a positive NHFR. The one exception is for the CA60 hole, where the horseshoe vortex on the upstream side of the hole is increasing the heat transfer coefficient in a region without much coolant present. This is avoided in the CA45 and CA30 cases, most likely because the horseshoe vortex has also mixed out some of the coolant from the jet, and the effectiveness levels are high enough to offset the augmentation.

At the higher blowing ratio of M=3.0, there are regions for each hole which exhibit negative NHFR, as observed in Figure 18b. HTC augmentation contours for these same cases were presented in Figure 14. The most significant region of negative NHFR in every case occurs to the side of the coolant jet downstream of x/D=5, where little coolant would be present, but where the streamwise vortex (or the CRVP for the CA0 hole) is augmenting the local heat transfer coefficient.

It is interesting to note that the region of negative NHFR on the leeward side of the jet downstream of x/D=5 increases in size and magnitude from CA15 to CA30, and then decreases from CA30 to CA60. Contours of heat transfer augmentation in Figure 14 show that augmentation monotonically increases from CA15 to CA60, so the higher NHFR in the CA45 and CA60 cases in Figure 18b is due to better lateral spread and attachment of coolant as the compound angle is increased.

Figure 19 shows the area-weighted average of NHFR from x/D=0-20, z'/D=±9 for all cases. This is a representation of the total reduction (or in some cases, increase) in heat flux over this entire area with the addition of film cooling. There is a clear trend of decreased heat flux reduction as blowing ratio increases. A trend within the compound angle cases with a common blowing ratio is not as clear, but the results are consistent with previously discussed augmentation and effectiveness data presented in Figure 16.

HTC augmentation increases with both compound angle and blowing ratio, so the fact that the same trend is not replicated for NHFR means that adiabatic effectiveness (Figure 16b) is playing an important role. Haydt and Lynch [1] showed that compound angled holes have two regimes: one from CA0-CA30 where effectiveness increases slightly with compound angle and decreases with blowing ratio, and one from CA45-CA60 where effectiveness remains high for all blowing ratios due to a wide spread of the coolant. These trends are reflected in the NHFR data in Figure 19. NHFR is slightly higher for CA15 than for CA0 at all blowing ratios, because the higher effectiveness offsets the slight increase in augmentation. As the compound angle is increased to CA30, however, the NHFR drops because the small increase in effectiveness cannot offset the significant increase in augmentation. CA45 and CA60 have similar adiabatic effectiveness but CA60 has the highest HTC augmentation, so its NHFR is lower. However, as the blowing ratio increases, the NHFR of the CA60 hole increases relative to the CA0-CA30 holes, since those holes experience a drop in effectiveness with blowing ratio. CA45 is the optimal configuration for high NHFR, since it has about the highest

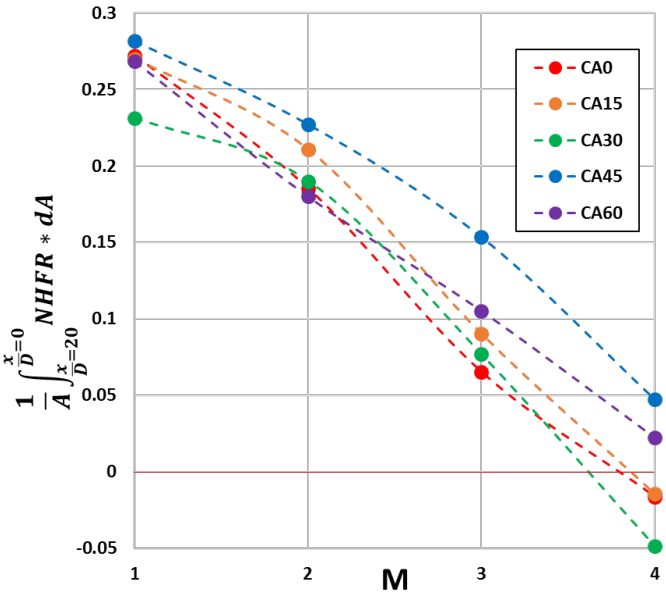

Figure 18: Area-weighted average of NHFR from x/D=0 to 20 for all tested cases, plotted versus blowing ratio.

adiabatic effectiveness, but does not have the highest HTC augmentation.

For the calculations of NHFR in Figure 19, a constant metal temperature of φ=0.6 is being used for all cases. This is not necessarily reflective of reality. As blowing ratio increases, in-hole convection would increase, and also internal back-side convection. Metal temperature would likely decrease with increasing blowing ratio, and therefore the drop in NHFR with blowing ratio might not be as severe as suggested here.

Comparison to Flowfield

Particle image velocimetry (PIV) measurements were collected for the same cases at the same blowing ratios and DR=1.0 by Haydt and Lynch [3]. The flowfield was measured at three downstream planes normal to the mainstream flow direction: x/D=0, 5, and 10. A comparison between the flowfield and the HTC augmentation is shown in Figure 20a for the CA0 hole, Figure 20b for the CA30 hole, and Figure 20c for the CA60 hole, all at M=3.0. Cross-planes at x/D=0, 5, and 10 are shown contoured with normalized x-vorticity (a transparent contour level indicates zero vorticity, large red regions indicate the streamwise vortex) and overlaid with in-plane velocity vectors. Data was not collected for a crossplane of x/D=10 for the CA30 case.

Figure 20 shows how the features of the flowfield influence the HTC augmentation. Starting in Figure 20a with a CA0 hole, the counter rotating vortex pair, indicated by the blue (negative x-vorticity) and red (positive x-vorticity) contour regions, causes very little flow inducement. The primary cause of HTC augmentation for this hole at the jet centerline is the attached coolant increasing the temperature gradient at the wall.

The streamwise vortex can be seen in Figure 20b for a moderate compound angle hole of CA30. The streamwise vortex is the large red region in the x-vorticity contour, located adjacent to the film cooling jet. This vortex induces in-plane velocity and sweeps fluid down to the wall and under the film cooling jet. For the crossplane of x/D=5 in Figure 20b, the streamwise vortex corresponds to a region of high HTC augmentation, where the in-plane flow is directed towards the endwall.

The strength and size of the streamwise vortex grows for the CA60 hole, depicted in Figure 20c, and with it the inducement of in-plane velocity. At the crossplanes of x/D=5 and 10, the streamwise vortex corresponds to a region of increased HTC, and the velocity vectors indicate that the flow is being driven down towards the wall and swept under the film cooling jet. The more significant in-plane velocity for the CA60 hole causes higher HTC augmentation than what was observed for the CA30 and CA0 case. Also, Figure 20c shows how the strong streamwise vortex of the CA60 hole persists downstream at a greater size and magnitude than the lesser compound angled holes, continuing to increase augmentation.

CONCLUSIONS

Shaped holes at a sweep of compound angles and a range of blowing ratios have been tested in order to determine HTC augmentation and NHFR. A thin foil which provides a constant

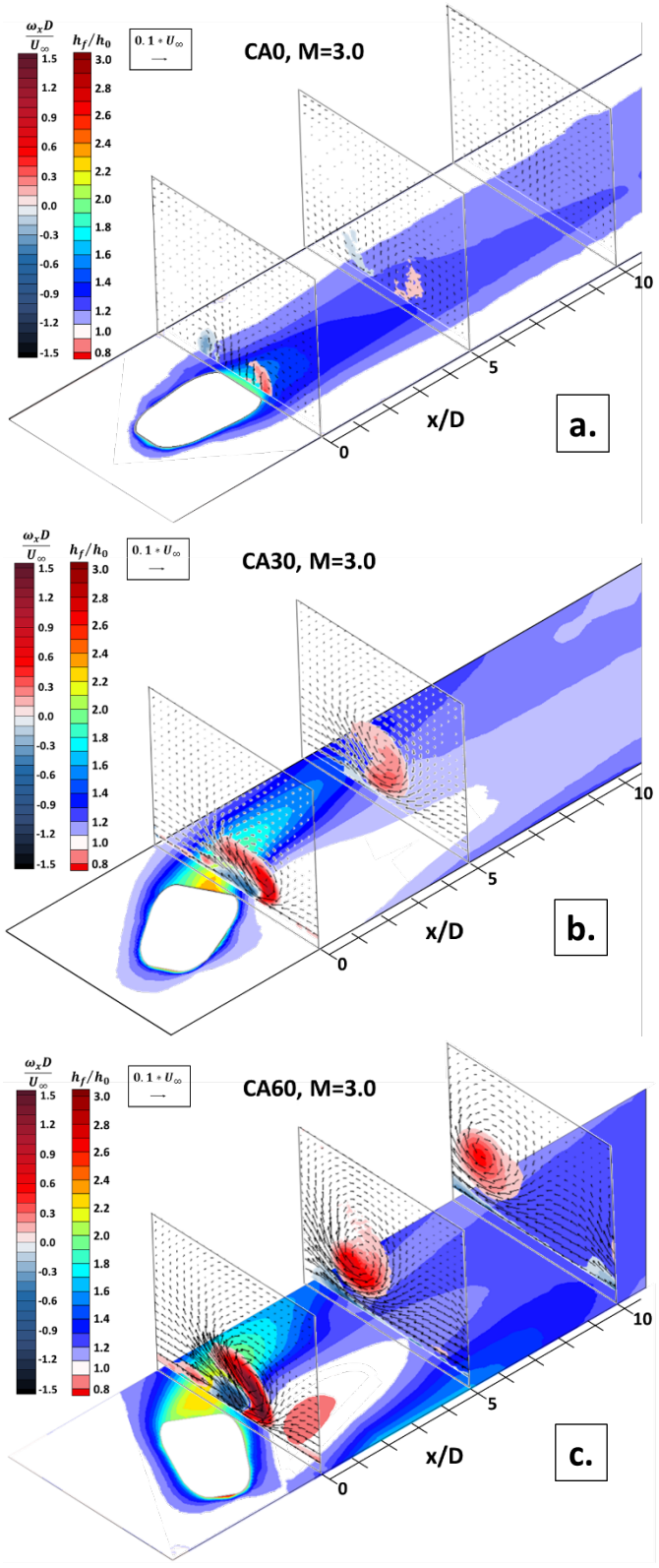

Figure 20: Experimental data for the a) CA0 hole, b) CA30 hole, and c) CA60 hole, all at M=3.0, showing HTC augmentation on the endwall and cross-planes contoured by normalized x-vorticity and overlaid with in-plane velocity vectors.

heat flux covers the extent of the test section, both upstream and downstream of the holes, with hole outlets cut out of the foil. Surface measurements were taken using infrared thermography and used to determine flat plate HTC, local heat flux, and HTC augmentation.

Laterally-averaged HTC augmentation increases monotonically with blowing ratio, and also increases with compound angle. There are four primary regions of HTC augmentation:

- A horseshoe vortex is formed at the leading edge of the film cooling hole due to the obstruction caused by the coolant jet. The size of this region and the magnitude of augmentation increase as compound angle increases, and thus the size of the obstruction.
- Also due to the obstruction of the jet, a region just downstream of the hole outlet is shielded from mainstream flow and has a reduced HTC relative to flat plate. This region also grows with increasing compound angle.
- The region of the coolant jet that remains attached to the wall and provides a high level of coolant concentration at the wall thins the boundary layer, which increases the HTC coefficient. The region over which this occurs increases in size with increasing compound angle, and also more coolant remains attached to the wall for high blowing ratios at large compound angles.
- The streamwise vortex induces mainstream flow that impinges on the endwall in the region adjacent to the jet, which increases HTC. This effect increases with increasing blowing ratio, as the flowfield becomes more asymmetric and the streamwise vortex gains strength.

Compound angled shaped holes can cause regions of negative NHFR, due to high augmentation existing in a region with low coolant concentration. Moderate compound angles from CA15-CA30 have increased HTC augmentation, but do not have significantly increased adiabatic effectiveness, so they have low NHFR. Higher compound angles from CA45-CA60 have the highest HTC augmentation, but also benefit from significant lateral spread of coolant, so the NHFR is higher especially at high blowing ratios. The hole with the highest NHFR is the CA45 hole, since it has very high adiabatic effectiveness, but has the least significant HTC augmentation.

ACKNOWLEDGMENTS

The authors are grateful to Pratt & Whitney, a United Technologies Corp. company, for their generous support of this project. We also would like to thank Phil Irwin for his skilled machining of all of the film cooling holes used in this study.

REFERENCES

[1] Haydt, S., and Lynch, S., 2018, "Cooling Effectiveness for a Shaped Film Cooling Hole at a Range of Compound Angles," ASME Turbo Expo, Lillestrom, Norway, ASME Paper GT2018-75726.

[2] Sen, B., Schmidt, D. L., and Bogard, D. G., 1996, "Film Cooling With Compound Angle Holes: Heat Transfer," ASME J. Turbomach., 118, pp. 800-807.

[3] Haydt, S., and Lynch, S., 2018, "Flowfield of a Shaped Film Cooling Hole over a Range of Compound Angles," ASME Turbo Expo 2018, Lillestrom, Norway, ASME Paper GT2018-75728.

[4] Schroeder, R. P., and Thole, K. A., 2014, "Adiabatic Effectiveness Measurements for a Baseline Shaped Film Cooling Hole," ASME Turbo Expo, Düsseldorf, Germany, ASME Paper GT2014-25992.

[5] Bunker, R. S., 2005, "A Review of Shaped Hole Turbine Film-Cooling Technology," Journal of Heat Transfer, 127(4), p. 441.

[6] Goldstein, R. J., Jin, P., and Olson, R. L., 1999, "Film Cooling Effectiveness and Mass/Heat Transfer Coefficient Downstream of One Row of Discrete Holes," ASME J. Turbomach., 121(2), pp. 225-232.

[7] Hay, N., Lampard, D., and Saluja, C. L., 1985, "Effects of Cooling Films on the Heat Transfer Coefficient on a Flat Plate With Zero Mainstream Pressure Gradient," Journal of Engineering for Gas Turbines and Power, 107(January), p. 6.

[8] Ammari, H. D., Hay, N., and Lampard, D., 1990, "The Effect of Density Ratio on the Heat Transfer Coefficient From a Film-Cooled Flat Plate," ASME J. Turbomach., 112(3), pp. 444-450.

[9] Baldauf, S., Scheurlen, M., Schulz, A., and Wittig, S., 2002, "Heat Flux Reduction From Film Cooling and Correlation of Heat Transfer Coefficients From Thermographic Measurements at Enginelike Conditions," ASME J. Turbomach., 124, pp. 699-709.

[10] Harrison, K. L., Dorrington, J. R., Dees, J. E., Bogard, D. G., and Bunker, R. S., 2009, "Turbine Airfoil Net Heat Flux Reduction With Cylindrical Holes Embedded in a Transverse Trench," ASME J. Turbomach., 131(1), p. 011012.

[11] Gritsch, M., Schulz, A., and Wittig, S., 2000, "Film-Cooling Holes With Expanded Exits: Near-Hole Heat Transfer Coefficients," International Journal of Heat and Fluid Flow, 21(2000), p. 10.

[12] Yu, Y., Yen, C. H., Shih, T. I. P., Chyu, M. K., and Gogineni, S., 2002, "Film Cooling Effectiveness and Heat Transfer Coefficient Distributions Around Diffusion Shaped Holes," Journal of Heat Transfer, 124(5), p. 820.

[13] Saumweber, C., and Schulz, A., 2012, "Free-Stream Effects on the Cooling Performance of Cylindrical and Fan-Shaped Cooling Holes," ASME J. Turbomach., 134(6), pp. 061007-061007-061012.

[14] Boyd, E. J., McClintic, J. W., Chavez, K. F., and Bogard, D. G., 2016, "Direct Measurement of Heat Transfer Coefficient Augmentation at Multiple Density Ratios," ASME J. Turbomach., 139(1), p. 011005.

[15] Aga, V., and Abhari, R. S., 2011, "Influence of Flow Structure on Compound Angled Film Cooling Effectiveness and Heat Transfer," ASME J. Turbomach., 133(3), pp. 031029-031029.

[16] Brauckmann, D., and von Wolfersdorf, J., 2005, "Influence of Compound Angle on Adiabatic Film Cooling Effectiveness and Heat Transfer Coefficient for a Row of Shaped Film Cooling Holes," ASME Turbo Expo 2005: Power for Land, Sea, and Air, ASME, Reno-Tahoe, Nevada, ASME Paper GT2005-68036.

[17] Anderson, J. B., McClintic, J. W., Bogard, D. G., Dyson, T. E., and Webster, Z. D., 2017, "Freestream Flow Effects on Film Effectiveness and Heat Transfer Coefficient Augmentation for Compound Angle Shaped Holes," ASME Turbo Expo 2017, Charlotte, NC, ASME Paper GT2017-64853.
[18] McClintic, J. W., Anderson, J. B., Bogard, D. G., Dyson, T. E., and Webster, Z. D., 2017, "Effect of Internal Crossflow Velocity on Film Cooling Effectiveness—Part II: Compound Angle Shaped Holes," ASME J. Turbomach., 140(1), pp. 011004-011010.
[19] Kays, W., Crawford, M. E., and Weigand, B., 2005, *Convective Heat and Mass Transfer*, McGraw-Hill.
[20] Figliola, R. S., and Beasley, D. E., 2006, *Theory and design for mechanical measurements*, John Wiley, Hoboken, N.J.
[21] Tyagi, M., and Acharya, S., 2003, "Large Eddy Simulation of Film Cooling Flow From an Inclined Cylindrical Jet," ASME J. Turbomach., 125(4), p. 734.
[22] Wright, L. M., Gao, Z., Varvel, T. A., and Han, J. C., 2005, "Assessment of Steady State PSP, TSP, and IR Measurement Techniques for Flat Plate Film Cooling," ASME Summer Heat Transfer Conference, San Francisco, California, ASME Paper HT2005-72363.